Alternative soot detection strategies for application in aero-engine test-beds: assessment of the performance and uncertainties of time-integrated LII

R. Roy[1], C. Blount[2], G. Ramesh[2], K. Ozanyan[2], P. Wright[2], V. Archilla[3], I.S. Burns[1*]
[1] Department of Chemical and Process Engineering, University of Strathclyde, Glasgow G1 1XJ, UK
[2] School of Electrical & Electronic Engineering, University of Manchester, Manchester, M1 3BB, UK
[3] Instituto Nacional de Técnica Aeroespacial (INTA), 28850 Torrejon de Ardoz (Madrid) ESPANA

Abstract
We describe a laser induced incandescence (LII) measurement system for 2D mapping of non-volatile particulate matter (soot) in full-scale aero-engine exhausts. Simulation allows us to quantify the sensitivity of the measurement to variation in physical properties such as primary particle size, over a range of laser fluences and as a function of beam diameter. We discuss the implications of our results for optimisation and calibration of soot imaging in exhaust streams.

Introduction

The impacts of particulate emissions from combustion processes on human-health and on the environment, including as an agent of climate change, are increasingly apparent. Strategies to reduce the environmental impact of aviation include developing new technology for future lower emissions, as well as attempting to reduce the environmental impact of existing systems. It is therefore essential for aircraft engine manufacturers to understand fully the emission profile of current and future engines and fuels (sustainable and modified fossil fuel) in order to meet existing and future regulations. An immediate challenge is to quantify non-volatile particulate matter (nvPM), i.e. soot, by non-intrusive exhaust measurements in full-scale aero-engine testing. The ability to perform such measurements routinely may ultimately guide technology developments to reduce emissions in future.
The International Civil Aviation Organisation (ICAO) defines NO_x, CO, UHC (unburnt hydrocarbons) and particulate matter emissions as the most harmful substances in the airport environment and requires manufacturers to certify the emission levels of these compounds in their new engines, demonstrating that they complied with specified maximum levels [1]. Non-volatile particle matter (nvPM) emissions, produced in the aviation sector, have been controlled by ICAO through the calculation of the smoke index or smoke number (SN) [1]. This procedure is based on the analysis of the reflectance loss of particles collected on filter paper from gas sampled from the engine exhaust. This test is carried out at engine testbeds under the operating conditions corresponding to the landing and take-off (LTO) cycle [2]. The smoke number is considered an outdated way of measuring soot content in exhausts. The extractive nature of its measurement is intrusive to the flow; it also lacks the sensitivity required to quantify low levels of particulate. Accordingly, the availability of a non-intrusive approach that could be used routinely during engine tests to image soot distribution in engine exhaust plumes would potentially lead to a step-change in the volume of data available to optimize engine performance for reduced emissions.

In this paper, we briefly describe a new experiment being implemented at the Spanish National Aerospace Centre (INTA) for Laser Induced Incandescence measurements in the exhaust plume of a full-scale aero-engine on a test-bed. We then describe the modelling of LII signal generation specific to this instrument, to assess the capabilities and limitations of the approach.

Experimental

The measurement system for 2D mapping of soot in aero-engine exhausts is illustrated in Figure 1. The requirements of a non-intrusive system is that no additional component impinges on the flow-field of the exhaust and entrained air. A scanned-beam approach will allow interrogation of the entire cross-section of the flow, whose diameter is up to 1.6m. The centre-line of the exhaust is approximately 6 m above the floor of the test cell, and 7 m from the side walls.

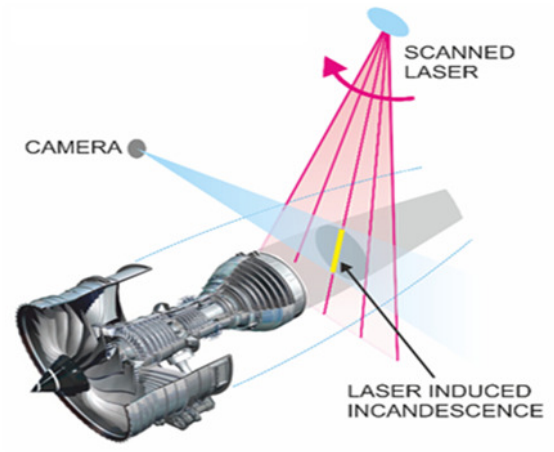

Figure 1: Illustration of the measurement approach for 2D mapping of soot

An Nd:YAG laser (Litron; wavelength: 1064 nm; peak power 800 mJ/pulse; pulse duration: 10 ns) is mounted (in a suitable protective housing) on a gantry roughly 3.5 m above the engine exhaust centre-line and the collimated beam is directed downwards by a scanning mirror. This causes the beam to sweep through a plane

* Corresponding author: iain.burns@strath.ac.uk

perpendicular to the exhaust flow direction. High laser-fluence is essential so that soot along the beam path is heated near to its sublimation temperature, thus maximising incandescence emission.
A non-intensified CCD camera (LaVision; integration time 2 μs) is mounted on the side wall of the test cell, as shown in Figure 2. The low level of particulate matter in the exhaust (soot volume fraction may be on the order of a part-per-billion) and the narrow collection solid-angle make it challenging to achieve the required sensitivity. To maximize the signal collected there is no spectral filtering on the camera. At a given moment, the LII signal is visible in images as a vertical streak.

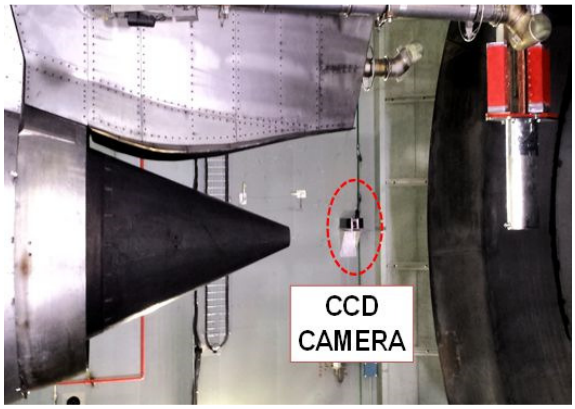

Figure 2: The engine exhaust and wall-mounted camera

There is no requirement to resolve spatial gradients on dimensions smaller than the beam diameter (~10 mm). Instead, the incandescence is integrated across the width of the imaged signal, as well as to a similar extent in the vertical direction. Auto-projection based image reconstruction will be performed to generate 2D maps of soot in the scanning plane.

Modelling of LII signals from exhaust plume

A model of LII signal generation underpins the measurements in the following respects: (i) to estimate uncertainties associated with time-integrated detection of LII signals and beam divergence; (ii) to optimise the experimental approach to minimise uncertainty and improve sensitivity. There is an extensive body of literature on modelling of LII signals, which cannot be discussed in detail here [3]. These models are based on mass and energy balances on a heated soot particle, taking account absorption, vaporisation, conduction and radiation. Some models also consider additional effects such as oxidation and desorption [4]. Some models also account for the effects of aggregation [5] or polydispersity of soot particles [6], although this requires further assumptions about the nature of particle morphology and size distribution. Previous extensive work Bladh et al [7] has estimated relative errors in LII signals at different particle sizes but for short (20 ns) gated detection of narrowband LII signals, both with prompt and delayed detection.

Our analysis here differs from previous work not so much in the physical basis of the model but in the application to the proposed exhaust plume measurements. As described above, the test-bed instrument involves a beam best approximated as having a Gaussian spatial profile, and signal collection that is temporally integrated and spectrally broad-band. The model predicts fluence curve, signals as a function of primary particle size, and signals as a function of beam diameter for this configuration of in-plume LII. It also allows estimation of absolute signal levels for the LII system, which serves as a test of feasibility given the low soot concentration in the exhaust and limited collection solid angle.

Energy balance

The LII model is based on an energy balance with the following terms:

$$Q_{int} = Q_{abs} - Q_{vap} - Q_{con} - Q_{rad} \qquad \textbf{(1)}$$

Where:
Q_{int} is the rate of change of internal energy of the soot particle;
Q_{abs} is the rate of absorption of laser energy by the soot particle;
Q_{vap} is the rate of energy loss through vaporisation;
Q_{con} is the rate of energy loss through conduction from the soot particle to the surrounding gas;
Q_{rad} is the rate of energy loss through radiation from the soot particle.

Internal Energy

The rate of change of energy stored by the particle is given by:

$$Q_{int} = c_{p\,s}\,\rho_s \left(\pi \frac{d_p^3}{6}\right) \frac{dT}{dt} \qquad \textbf{(2)}$$

Where $c_{p\,s}$ and ρ_s are the specific heat and density of soot d_p is the primary particle size of soot.

Rate of absorption

The rate of absorption depends on the absorption cross section, C_{abs}, and the fluence temporal profile, $F(t)$. The absorption term is based on:

$$Q_{abs} = C_{abs}\,F(t) \qquad \textbf{(2)}$$

As the soot is considered mature an absorption function, $E(m)$, of 0.36 was chosen. Typically for mature soot it has been stated that a value of 0.35 to 0.4 should be used [8].

Rate of Conduction

Conduction occurs by energy being lost at the particle surface due to collisions with gas molecules. The rate of conduction has been evaluated using the McCoy and Cha method [3]:

$$Q_{Con} = \frac{2\pi\, d_p^2\, k_g \left(T_p(i) - T_g\right)}{d_p + G\, \lambda_{mfp}} \quad \textbf{(3)}$$

Where k_g is the gas heat transfer coefficient, G is the geometry heat transfer, and λ_{mfp} is the mean free path. T_p is the particle temperature and T_g is the gas temperature.

Rate of evaporation

At higher fluences the particles reach high enough temperatures to cause evaporation. Evaporation not only causes cooling but also mass-loss and thus reduction in particle diameter. The energy lost through evaporation is dependent on the enthalpy of vaporisation of soot and the rate at which the mass is lost [8]:

$$Q_{Vap} = -\frac{\Delta H_{Vap}}{M_{SV}} \frac{dm_p}{dt} \quad \textbf{(4)}$$

Where ΔH_{Vap} is the enthalpy of vaporisation of soot, M_{sv} is the molar mass of soot vapour and m_p is the mass of the soot particle.

Mass change during evaporation can be described by a mass balance using the equations from:

$$\frac{dm_p}{dt} = -\pi\, d_p^2\, N_{SV}\, \frac{M_{SV}}{N_A} \quad \textbf{(5)}$$

Where N_A is the Avogadro number and N_{SV} is the molecular flux.

Radiation

Radiation is generally makes only a minor contribution to the heat balance, other than at sub-atmospheric pressure but is responsible for signal generation. To account for loss by radiation the model uses Planck's black-body equation integrated over all solid angles and wavelengths [9]:

$$Q_{Rad} = \frac{\left(199\, \pi^3 d_p^3\right)\left(k_B\, T_p\right)^5\, E(m)}{h\, (h\, c)^3} \quad \textbf{(1)}$$

Where k_B is Boltzmann's constanst, c is the speed of light and h is Planck's constant

Accordingly, the LII signal at a given wavelength, λ_s, as:

$$S = \frac{8\, \pi\, d_p^3\, h\, c^2\, E(m)}{\lambda_s^6 \left[\left(\exp\left(\frac{h\, c}{\lambda_s\, k_B\, T_p(t)}\right)\right) - 1\right]} \quad \textbf{(7)}$$

Signal integration

The signal thus calculated is for one individual primary particle. To determine the overall signal, the number (N) of monodisperse particles in the measurement volume needs to be found for a given soot volume fraction (f_V).

$$N = \frac{(f_v V_{measurement})}{d_p} \quad \textbf{(8)}$$

The model also predicts the signal at a given detection wavelength, for a specific laser fluence and for a given particle temperature. To determine the collected signal for our experimental approach, we must integrate:

i. Spectrally, taking account of the spectral efficiency curve of the camera;
ii. Temporally, since the camera has a long exposure time (2 μs)
iii. Radially, since the laser spatial profile isn't top-hat.

The simulation involves a time-stepping solution, which keeps track of the particle temperature and mass. Therefore, at each time-step, the signal can be calculated at a range of discrete wavelengths. A spectral sensitivity plot for the camera was available from the manufacturer's specification sheet (LaVision). The spectral quantum efficiency of the camera is the probability of a count being recorded and is wavelength dependent.

Only a small fraction of the emitted LII signal reaches the detector. The collection solid angle was estimated based on the distance from the centre of the exhaust plume to the camera and the diameter of the lens. This allows for the signal to be converted to counts registered by the camera. This process was followed for each time-step, allowing the temporally integrated signal to be determined in the form of counts on the detector.

The local fluence at radial position r in a beam with a Gaussian spatial profile is given by [8]:

$$F(r) = \frac{P}{f} \frac{2}{\pi\, r_L^2}\ \exp\left(-\frac{r^2}{\omega_2^2}\right) \quad \textbf{(9)}$$

Where $F(r)$ is the local laser fluence at position r in the beam, P is the average laser power, f is the pulse frequency, r_L is the laser beam radius. Time-integrated, broad-band signals were calculated as described above for the prevailing fluence in each annular region of the beam. These calculated signals were then integrated radially to determine the overall incandescence generated over the width of the beam.

Model Results

Since the detection is time-integrated, the signal is dependent on the rate of cooling and thus on the primary particle size. This dependence is shown in Figure 3. Since aero-engines may produce different particle sizes depending on the engine regime, it is important to understand the sensitivity of the overall signal to

variation in particle size [7], which may be roughly in the range 20-30 nm for representative aircraft soot [10]. For this range of 20-30 nm primary particle size, the results in Fig 1 show a variation of around ±20% in the predicted integrated LII signal for a soot volume fraction of 2 ppb and a beam diameter of 12 mm ($1/e^2$). This uncertainty could be narrowed if an *a priori* relationship between engine load and expected particle size could be estimated, for example by time-resolved LII measurements on the exhaust of a smaller, but representative, engine.

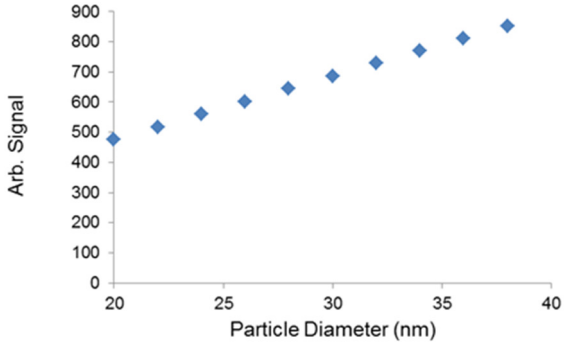

Figure 3: Simulated dependence of time-integrated LII signal on primary particle diameter for a pulse energy of 0.6 J

The time-resolved LII profiles for particles near to the maximum and minimum of this size-range can be seen in Figure 4Figure . For the smaller particle, a faster rate of cooling is observed and leads to a lower signal for time-integrated detection.

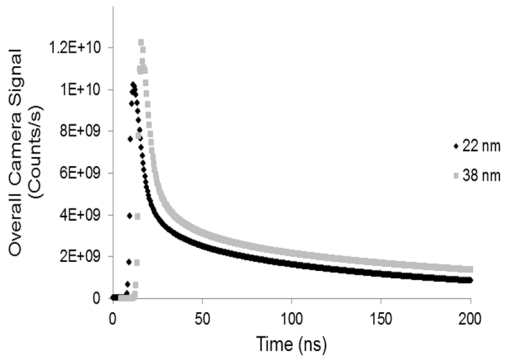

Figure 4: Time resolved profiles of two different particle sizes at pulse energy of 0.6 mJ

Fluence curves were also simulated for time-integrated LII and are shown in Figures 5 and 6. Figure 5 shows the calculated fluence curves for two different particle sizes, with a more extreme variation in size than described previously. The normalised fluence curves shown illustrate that the particle size appears to have little impact on the shape of the fluence curve, with a fairly flat plateau in each case.

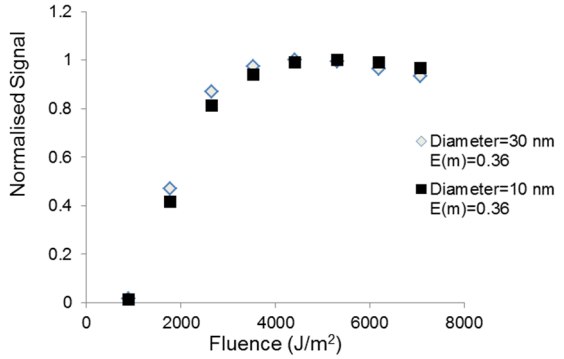

Figure 5: Fluence curves (based on the $1/e^2$ diameter of 12 mm) at two different particle sizes

Figure 6 shows without normalisation the effect of particle size and $E(m)$ on the fluence curve. As expected the smaller particles are associated with a lower signal due to faster cooling. It should be emphasised that the variation in particle size shown here is exaggerated to illustrate this difference.

The fluence curve for the larger absorption function, $E(m)$, shows a higher signal than the modelled signal at lower absorption function. This is mainly related to the amount of light the soot particle emits through the radiation term as discussed earlier: radiation is proportional to $E(m)$. Additionally, we see that the fluence curve for the higher $E(m)$ case acquires a more noticeable negative gradient for high fluences. This is due to the additional energy absorption

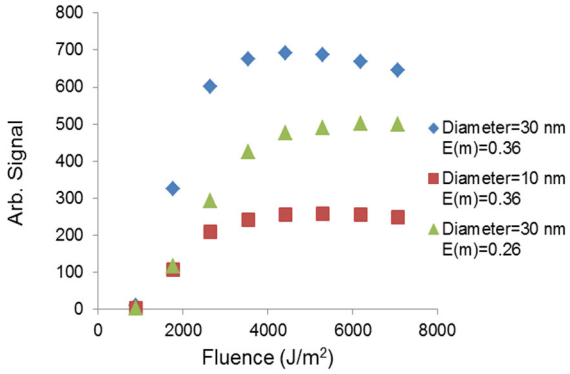

Figure 6: Fluence curves (based on the $1/e^2$ diameter of 12 mm) simulated for different particle diameters and values of absorption function

The fluence curves also depend on the initial temperature of the particle and the gas so work is currently underway to investigate how the fluence curve is changed with variation in the surrounding gas temperature.

The model was also be used to predict how the signals detected by the camera will vary as a function of the laser beam diameter for given pulse energy. Changing the beam diameter in the model alters the local fluence as well as the overall measurement volume.

Simulations were performed for the maximum laser pulse energy of 0.8 J. Figure 7, presents the overall

signal integrated across the width of the projected image of the illuminated region on the camera. Initially, increases in beam diameter result in higher overall signal, since signal is generated over a larger volume and there is still enough energy to raise the particles to a high temperature. Successive increases in beam waist eventually lead to reduced signal due to lower peak particle temperature. All of this is a consequence of the non-linear nature of the technique (in contrast to laser-induced fluorescence, for example). It can be seen that to maximise the LII signal integrated spatially across the measurement volume, the diameter of the beam can increased to 16 mm ($1/e^2$).

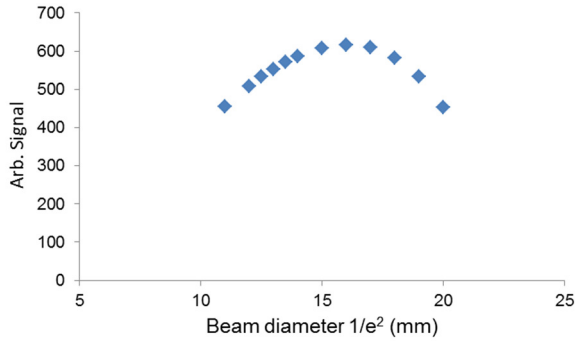

Figure 7: Overall spatially integrated signal across the measurement volume at a pulse energy of 0.8 J, as a function of beam diameter

This has implications not only in selecting the beam diameter to use for measurements, but also in understanding the effects of beam divergence in the plume due to turbulence.

Conclusions

Modelling of LII signal generation was used to assess the performance of a measurement system for 2D mapping of non-volatile particulate matter in aero-engine exhausts. Detected LII signals were simulated to estimate the uncertainty in using time-integration detection to measure soot volume fraction. Time-resolved LII profiles were also shown for the instrument configuration described. Calculated fluence curves to show that while particle size doesn't influence the overall shape of the fluence curve is does affect the absolute signal. The effect of beam diameter on integrated LII signal has been investigated, with implications in optimising instrument performance.

Acknowledgements

This work is part of the CIDAR Project (Combustion species Imaging Diagnostics for Aero-engine Research) and supported by European Union's Horizon 2020 Research and Innovation Framework Programme under grant agreement No 785539. The authors are grateful for useful discussions with Mark Johnston and John Black.

References

[1] International Civil Aviation Organisation(2008), Environmental Protection:Internation Standards and Recommended Practices- Annex 16 to the convention on internaitonal civil aviation, Montreal, Canada: Taylor & Francis, 2016.

[2] OACI Doc, "9889 Airpit Air Quality Manual," 2011.

[3] H. A. Michelsen, B. Kock, F. Liu, H. Bladh, A. Boiarciuc, M. Charwatch, T. Dreier, R. Hadef, M. Hofmann, J. Reimann, S. Will, P. Bengtsson, H. Bockhorn, F. Foucher, K. Geigle, R. Stirn, B. Tribalet and R. Suntz, "Modelling laser-induced incandescence : a summary and comparison of LII modles," *Applied physics B,* pp. 503-521, 2007.

[4] H.A.Michelsen, "Understanding and predicing the temporal response of laser-induced incandescence from carbonaceous particles," *Journal of Chemical Physics,* p. 7012, 2003.

[5] F. Liu and G. J. Smallwood, "Effect of aggregation on the absorption cross-section of fractal soot aggregates and its impact on LII," *Journal of Quantitative Spectroscopy and Radiative Transfer,* vol. 111, no. 2, pp. 302-308, 2010.

[6] R. P. Bambha and H. A. Michelsen, "Effects of aggregate morphology and size on laser-induced incandescence and scattering from black carbon (mature soot)," *Journal of Aerosol Science,* vol. 88, pp. 159-189, 2015.

[7] H. Bladh, J. Johnsson and P. Bengtsson, "On the dependence of the laser-induced incandescence (LII) signal on soot volume fraction for variations in particle size," *Applied Physics B,* vol. 90, no. 1, pp. 109-125, 2007.

[8] H. Bladh and P. E. Bengtsson, "Characteristics of laser-induced incandescence from soot in studies of a time-dependant," *Applied Physics B: Lasers and Optics,* vol. 78, no. 2, pp. 241-248, 2004.

[9] C. Schulz, B. Kock, M. Hofmann, H. A. Michelsen, S. Will, B. Bougie, R. Suntz and G. J. Smallwod, "Laser-induced incandescence:recent trends and current questions," *Applied Physics B: Laser and Optics,* vol. 83, no. 3, pp. 333-354, 2006.

[10] M. Stettler, J. Swanson, R. H. Barrett and A. M. Boies, "Updated correlation between aircraft smoke number and black carbon concentration," *Aerosol Science and Technology ,* vol. 47, no. 11, pp. 1205-1214, 2013.